

MEAN FIELD CONTROL PROBLEMS FOR VACCINE DISTRIBUTION*

WONJUN LEE [†], SITING LIU[†], WUCHEN LI [‡], AND STANLEY OSHER[†]

Abstract. With the invention of the COVID-19 vaccine, shipping and distributing are crucial in controlling the pandemic. In this paper, we build a mean-field variational problem in a spatial domain, which controls the propagation of pandemic by the optimal transportation strategy of vaccine distribution. Here we integrate the vaccine distribution into the mean-field SIR model designed in [25]. Numerical examples demonstrate that the proposed model provides practical strategies in vaccine distribution on a spatial domain.

Key words. Mean-field Controls, Vaccine, Epidemics, Primal-dual algorithm.

AMS subject classifications. 91C20

1. Introduction. The COVID-19 pandemic has affected society significantly. Various actions are taken to mitigate the spread of the infections, such as travel ban, social distancing, and mask-wearing. The recent invention of the vaccine yields breakthroughs in fighting against this infectious disease. According to the media, different vaccines, including Pfizer, Moderna, and Janssen (J&J) report that their vaccines show approximately 66%-95% efficacy at preventing both mild and severe symptoms of COVID-19. Therefore, the deployment of COVID-19 vaccines is an urgent and timely task. Many countries have implemented phased distribution plans that give the elderly and healthcare workers priority to get vaccinated. Meanwhile, the shipping and distribution of the vaccine are expensive due to the cold chain transportation. An effective distribution strategy is necessary to eliminate infectious disease and prevent more death.

In this work, we propose a novel mean-field control model based on [25]. In our model, there are two types of approaches (controls) that can be used to control the pandemic: movement of populations and vaccine distribution strategy. The first one has been discussed thoroughly in [25], where we address the spatial effect in pandemic modeling by introducing a mean-field control problem into the spatial SIR model. By applying spatial velocity into the classical disease model, the different populations (susceptible, infected, and recovered) are moved accordingly hence controlling the epidemic's propagation. We considered several aspects of the vaccine in our model as for vaccine distribution, including manufacturing, delivery, and consumption. With limited vaccine supply, we aim at finding an optimal vaccine distribution strategy: *when and where to deliver?* Our goal is to find a strategy to move the population and distribute vaccines to minimize the total number of infectious, the amount of movement of the people, and the transportation cost of the vaccine with limited vaccine supply. To tackle this question, we ensemble these two controls and propose the following constrained optimization problem:

$$\min \mathcal{P}((\rho_i, v_i)_{i \in \mathbb{S}}, f) = \mathcal{E}_{final}(\rho_i(T, \cdot)_{i \in \{S, I, R\}}) + \mathcal{E}_{running}((\rho_i, v_i)_{i \in \mathbb{S}}, f)$$

*Submitted to the editors April 27, 2021

Funding: This work is supported by AFOSR MURI FA9550-18-1-0502.

[†]Department of Mathematics, University of California, Los Angeles (wlee@math.ucla.edu, siting6@math.ucla.edu, sjo@math.ucla.edu.)

[‡]Department of Mathematics, University of South Carolina (wuchen@mailbox.sc.edu)

subject to

$$\begin{cases} \partial_t \rho_S + \nabla \cdot (\rho_S v_S) = -\beta \rho_S K * \rho_I + \frac{\eta_S^2}{2} \Delta \rho_S - \theta_1 \rho_V \rho_S & (t, x) \in (0, T) \times \Omega \\ \partial_t \rho_I + \nabla \cdot (\rho_I v_I) = \beta \rho_S K * \rho_I - \gamma \rho_I + \frac{\eta_I^2}{2} \Delta \rho_I & (t, x) \in (0, T) \times \Omega \\ \partial_t \rho_R + \nabla \cdot (\rho_R v_R) = \gamma \rho_I + \frac{\eta_R^2}{2} \Delta \rho_R + \theta_1 \rho_V \rho_S & (t, x) \in (0, T) \times \Omega \\ \partial_t \rho_V = f(t, x) - \theta_2 \rho_V \rho_S & (t, x) \in (0, T') \times \Omega \\ \partial_t \rho_V + \nabla \cdot (\rho_V v_V) = -\theta_2 \rho_V \rho_S & (t, x) \in [T', T] \times \Omega \end{cases}$$

and

$$\begin{cases} 0 \leq f(t, x) \leq f_{max} & (t, x) \in [0, T'] \times \Omega_{factory} \\ f(t, x) = 0 & (t, x) \in [0, T'] \times \Omega \setminus \Omega_{factory} \\ \rho_V(t, x) \leq C_{factory} & (t, x) \in [0, T'] \times \Omega_{factory} \end{cases}$$

In our model, different populations are described using $\rho_i, i \in \{S, I, R\}$, representing the susceptible, infectious, and recovered. The term $\rho_V(x, t)$ describes the density distribution of the vaccine over the spatial domain at location x and time t . The control variables $v_i, i \in \{S, I, R\}$ create a velocity field over time-space domain that move the corresponding populations. As for vaccines, the control variable v_V represents the vaccine's transportation strategy, and the control variable $f(t, x)$ describes how many vaccines are produced at a specific time and location. In the optimization objective function, \mathcal{E}_{final} represents the goal of our control to achieve at the terminal time, such as minimizing the total number of infectious individuals and maximizing the total number of recovered (immune) persons. $\mathcal{E}_{running}$ represents the running cost, including transportation of vaccines, movement of the different class of the population, etc. We will discuss more details on the choice of the cost in the modeling section. As for constraints of our optimization problem, the five partial differential equations of $\rho_i, i \in \{S, I, R, V\}$ describe the dynamics of the different class of population and vaccines in terms of density. The inequalities of $f(t, x)$ models the limitation of vaccine manufacturing. The vaccine is only produced at some particular factory location $x \in \Omega_{factory}$ and a daily maximal rate of f_{max} . The dynamic of the vaccine density ρ_V shares some similar aspects to the unnormalized optimal transport[24]. Specifically, they both study the transportation of mass while there is a source term that is creating mass.

Due to the multiplicative interaction terms : $\rho_S K * \rho_I, \rho_I K * \rho_S, \rho_V \rho_S$, the constrained optimization problem is non-convex. Hence we introduce Lagrange multipliers to formulate it as an unconstrained optimization problem. However, it also introduces a major computational challenge due to the high dimensionality of the problem brought by the Lagrange multipliers. We handle it efficiently via a first-order Primal-Dual Hybrid Gradient (PDHG) method. Specifically, we apply its variant, generalized proximal (G-prox) PDHG[18], with a suitable choice of variable norms to achieve a convergence rate independent of the finite-difference mesh size.

Lots of mathematical models are invented to predict the future of COVID-19 epidemics. Recently proposed models take more real-world situations into considerations and tend to be more effective in quantitative forecasting. Specifically, there have been studies on the impact of actions such as locked down, social distancing, wearing a mask [11, 10, 14]. Data-driven approach and machine learning techniques are also

integrated to estimate the parameters for the epidemic better and boost the prediction of the trend of the pandemic model [30, 28]. Meanwhile, optimal control serves as an important tool in pandemic control. They seek the optimal strategy to minimize the total number of infected people while keeping some form of costs at a minimum. There are work focus on mitigating the epidemic with limited medical supply, such as ICU capacity [8], face masks [27] and vaccines [33, 16, 21, 26, 19]. In [19], an optimal vaccine distribution strategy is proposed with a limited total amount of vaccines and maximal daily supply. [26] first uses inverse problem to determine the parameters of the SIR model. Then it formulates two optimal control problems, with mono- and multi-objective, and solve for the optimal strategy of vaccine administration. Other non-pharmaceutical interventions are also considered in the scope of optimal control of epidemics, including social distancing, closing schools, and lockdowns [15, 20, 31]. [20] computes the optimal non-pharmaceutical intervention strategy based on an extended SEIR model with the absence of the vaccine. The mean-field control problem can be viewed as a particular type of optimal control, where the control is applied to an individual in terms of population density.

Mean-field game (control), introduced by [17, 23], describes the deterministic (stochastic) differential games as the number of players tends to infinity, where a given player interacts through the distribution of all players in the state-space. It is a thriving research direction with applications in economics, crowd motion, industrial engineering, and more, including epidemics [12, 3, 22]. Numerical methods are also invented to obtaining quantitative information of such mean-field game(control) models, especially when the state-space is in high dimensions [1, 2, 5, 29]. Multi-population mean-field game(control) problems have also draw lots of attention [13, 9, 4]. This type of problem studies the interactions in two levels: between agents of the same population and between populations. Our model is indeed a multi-population mean-field control problem, with population dynamic is described using reaction-diffusion equations adopted from the SIR model. Here, our optimization's constraints come from two perspectives: the dynamic of each population and the density evolution of vaccine, which are all described as continuity equations; the limited supply of the vaccine. Therefore, we obtain a novel mean-field control problem.

The rest of the paper is organized as follows. In Section 2, we propose a novel multi-population mean-field control model and explain how the population movement and vaccine distribution are integrated into a constrained optimization problem. We discuss, in Section 3, the challenges in numerically solving this mean-field control model and propose a first-order primal-dual algorithm to solve it. We present numerical experiments with different model parameter choices and discuss their implications on mean-field controls in Section 4. In Section 5, we present concluding remarks and discuss potential directions.

2. Models. In this section, we review the classical SIR model. Based on it, we formulate the spatial SIR dynamics with vaccine distribution, namely SIRV dynamics. We then introduce a variational problem to control the SIRV dynamics.

2.1. Classical SIR model. The SIR models an infectious disease epidemic via an ordinary differential equation system

$$\begin{cases} \frac{dS}{dt} = -\beta IS \\ \frac{dI}{dt} = \beta IS - \gamma I \\ \frac{dR}{dt} = \gamma I. \end{cases}$$

The population is divided into three classes: susceptible, infected and recovered. While assuming a closed population without births or deaths, the model uses $S(t)$, $I(t)$ and $R(t)$ to represent the number in each compartment at the time t . The SIR model has two parameters: β is the effective contact rate of the susceptible individual gets infected; γ is the recovery rate of the infected individual. The simplicity of this model allows people to predict an infectious disease epidemic by only estimating a few parameters. However, it has limitations by assuming the population is homogeneous-mixing, which means that every individual has an equal probability of disease-causing contacts. As a result, the predictions will lack spatial information and may not help the (local) governments make policy or relocate medical resources. Therefore, we are motivated to study the spatial SIR model. On the other hand, the SIR model does not consider the latent period between when a person is exposed to a disease and when he/she becomes infected. This leads to the extension of the SIR model, such as the SEIR model. Our proposed model has a flexible structure and can be generalized to such pandemic models naturally.

2.2. Spatial SIR variational problem with vaccine distribution. In [25], we add the spatial dimension to the S , I , R functions. Let $\Omega \subset \mathbb{R}^d$ be a bounded domain. Consider the following density functions

$$\rho_S, \rho_I, \rho_R : [0, T] \times \Omega \rightarrow [0, \infty).$$

Here, ρ_S , ρ_I , and ρ_R represent susceptible, infected, and recovered populations distribution, respectively. We assume ρ_i for each $i \in \{S, I, R\}$ moves over a spatial domain Ω with velocity v_i . Here $v_i, i \in \{S, I, R\}$ are our controls variables. With a change of variable $m_i = \rho_i v_i, i \in \{S, I, R\}$, we define momentum vector fields

$$m_S, m_I, m_R : [0, T] \times \Omega \rightarrow \mathbb{R}^d$$

that govern the corresponding density flows. In the following, instead of using control variable v_i , we replaced it with $\frac{m_i}{\rho_i}, i \in \{S, I, R\}$ and regard m_i as the control variable.

We can describe the flows of the densities by the following continuity equations.

$$(2.1) \quad \begin{cases} \partial_t \rho_S + \nabla \cdot m_S = -\beta \rho_S K * \rho_I + \frac{\eta_S^2}{2} \Delta \rho_S \\ \partial_t \rho_I + \nabla \cdot m_I = \beta \rho_I K * \rho_S - \gamma \rho_I + \frac{\eta_I^2}{2} \Delta \rho_I \\ \partial_t \rho_R + \nabla \cdot m_R = \gamma \rho_I + \frac{\eta_R^2}{2} \Delta \rho_R \\ \rho_S(0, \cdot), \rho_I(0, \cdot), \rho_R(0, \cdot) \text{ are given.} \end{cases}$$

This system of continuity equations describes the flows of three groups of densities while satisfying the SIR model. The nonnegative constants η_i ($i \in \{S, I, R\}$) are the

coefficients for viscosity terms and $K = Kx$ is a symmetric positive definite kernel with $(K * \rho)(x, t) = \int_{\Omega} Kx\rho(y, t) dy$. In this model we consider the Gaussian kernel

$$Kx = \frac{1}{\sqrt{(2\pi)^d}} \prod_{k=1}^d \frac{1}{\sigma_k} \exp\left(-\frac{|x_k - y_k|^2}{2\sigma_k^2}\right).$$

The kernel convolution describes the spreading rate of the infectious disease over the spatial domain. In addition, we assume the Neumann boundary conditions on $\partial\Omega$. Since we don't consider birth or death in our model, the total population is conserved, which leads to the following equality

$$\frac{\partial}{\partial t} \int_{\Omega} \rho_S(t, x) + \rho_I(t, x) + \rho_R(t, x) dx = 0, \quad t \in [0, T].$$

In this paper, we consider the optimization problem for the distribution of vaccines. We add an extra function $\rho_V : [0, T] \times \Omega \rightarrow [0, \infty)$ which represents the vaccine density in Ω at each time $t \in [0, T]$. The PDE of the vaccine distribution will be described as the following PDE:

$$(2.2) \quad \begin{aligned} \partial_t \rho_V &= f(t, x) - \theta_2 \rho_V \rho_S & t \in (0, T') \\ \partial_t \rho_V + \nabla \cdot m_V &= -\theta_2 \rho_V \rho_S & t \in [T', T], \quad 0 < T' < T. \end{aligned}$$

where $m_V : [T', T] \times \Omega \rightarrow \mathbb{R}^d$ is a momentum vector field, θ_2 represents the utilization rate of vaccines and $f : (0, T') \times \Omega \rightarrow [0, \infty)$ represents the production rate of vaccines in $x \in \Omega$ at $0 < t < T'$. During $0 < t < T'$, the vaccines are produced with a production rate of f and used at a rate of $\theta_2 \rho_V \rho_S$. During $T' \leq t < T$, the vaccines are delivered to the area where the susceptible population is located, and they are used at a rate of $\theta_2 \rho_V \rho_S$. In summary, the first part of the PDE describes vaccines' production, and the second part describes the delivery of vaccines. For all time $0 < t < T$, the susceptible population are vaccinated if the vaccines are available in the same area. Now we are ready to introduce the new system of equations for the SIRV model.

$$(2.3) \quad \left\{ \begin{aligned} \partial_t \rho_S + \nabla \cdot m_S &= -\beta \rho_S K * \rho_I + \frac{\eta_S^2}{2} \Delta \rho_S - \theta_1 \rho_V \rho_S & (t, x) \in (0, T) \times \Omega \\ \partial_t \rho_I + \nabla \cdot m_I &= \beta \rho_S K * \rho_I - \gamma \rho_I + \frac{\eta_I^2}{2} \Delta \rho_I & (t, x) \in (0, T) \times \Omega \\ \partial_t \rho_R + \nabla \cdot m_R &= \gamma \rho_I + \frac{\eta_R^2}{2} \Delta \rho_R + \theta_1 \rho_V \rho_S & (t, x) \in (0, T) \times \Omega \\ \partial_t \rho_V &= f(t, x) - \theta_2 \rho_V \rho_S & (t, x) \in (0, T') \times \Omega \\ \partial_t \rho_V + \nabla \cdot m_V &= -\theta_2 \rho_V \rho_S & (t, x) \in [T', T] \times \Omega \\ \rho_S(0, \cdot), \rho_I(0, \cdot), \rho_R(0, \cdot), \rho_V(0, \cdot) & \text{ are given.} \end{aligned} \right.$$

In the first and third equation, we added the terms $+\theta_1 \rho_V \rho_S$ and $-\theta_1 \rho_V \rho_S$, respectively. The constant θ_1 represents the vaccine efficiency and $\theta_1 \rho_V(t, x) \rho_S(t, x)$ represents the vaccinated population at $(t, x) \in (0, T) \times \Omega$. We denote a set $\mathbb{S} = \{S, I, R, V\}$

and define a nonlinear operator A as follows

$$\begin{aligned}
(2.4) \quad A((\rho_i, m_i)_{i \in \mathbb{S}}, f) := & (\partial_t \rho_S + \nabla \cdot m_S - \frac{\eta_S^2}{2} \Delta \rho_S + \beta \rho_S K * \rho_I + \theta_1 \rho_S \rho_V, \\
& \partial_t \rho_I + \nabla \cdot m_I - \frac{\eta_I^2}{2} \Delta \rho_I - \beta \rho_S K * \rho_I + \gamma \rho_I, \\
& \partial_t \rho_R + \nabla \cdot m_R - \frac{\eta_R^2}{2} \Delta \rho_R - \gamma \rho_I - \theta_1 \rho_S \rho_V, \\
& \partial_t \rho_V - f \mathcal{X}_{[0, T']}(t) + \nabla \cdot m_V \mathcal{X}_{[T', T]}(t) + \theta_2 \rho_S \rho_V),
\end{aligned}$$

where \mathcal{X}_C is a step function that equals 1 on C and 0 otherwise.

The cost functional we propose in this paper is the extension of our previous paper [25]. We design the minimizers (ρ_i, m_i) , $i \in \mathbb{S}$ of the total cost functional, which is to:

- (i) minimize the transportation cost for moving each population;
- (ii) minimize the total number of infected people and the total number of susceptible people by maximizing the usage of the vaccines at time T ;
- (iii) maximize the total number of recovered people at time T ;
- (iv) avoid high concentration of population and vaccines at each time $t \in (0, T)$;
- (v) minimize the amount of vaccines produced during $t \in (0, T')$;
- (vi) minimize the transportation cost for delivering vaccines during $t \in (T', T)$.

Item (i) can be described by

$$\int_0^T \int_{\Omega} F_i(\rho_i(t, x), m_i(t, x)) dx dt,$$

for $i \in \{S, I, R\}$ where

$$(2.5) \quad F_i(\rho_i, m_i) = \begin{cases} \frac{\alpha_i |m_i|^2}{2\rho_i} & \text{if } \rho_i > 0 \\ 0 & \text{if } \rho_i = 0 \text{ and } |m_i| = 0 \\ \infty & \text{if } \rho_i = 0 \text{ and } |m_i| > 0. \end{cases}$$

The parameter α_i characterizes the cost of moving ρ_i with velocity $\frac{m_i}{\rho_i}$. Larger α_i means it is more expensive to move ρ_i . Note that this function comes from the quadratic kinetic energy. To see this, we use the definition $m_i = \rho_i v_i$ and plug into the formula,

$$F(\rho_i, v_i) = \frac{\alpha_i}{2} \rho_i |v_i|^2.$$

Item (ii) and (iii) can be described by the terminal costs of the cost functionals

$$\begin{aligned}
\mathcal{E}_i(\rho_i(T, \cdot)) &= \int_{\Omega} e_i(\rho_i(T, x)) dx \quad (i = S, I, V), \\
\mathcal{E}_R(\rho_R(T, \cdot)) &= \int_{\Omega} e_R(1 - \rho_R(T, x)) dx,
\end{aligned}$$

where a function $e : [0, \infty) \rightarrow [0, \infty)$ is a convex function. We also minimize the terminal cost for ρ_V because maximizing the usage of vaccines is equivalent to minimizing the number of vaccines left at the terminal time T . The total number of the recovered can be maximized by penalizing the density at the terminal time if the

value of $\rho_R(T, x)$ is far away from 1 for $x \in \Omega$. In this paper, we use a quadratic cost function

$$e_i(t) = \frac{a_i}{2} t^2, \quad (t \in [0, \infty))$$

where a_i is some constant.

Item (iii) can be described by the terminal costs of the cost functional

$$\mathcal{E}_i(\rho_i(T, \cdot)) = \int_{\Omega} e_i(\rho_i(T, x)) dx \quad (i = S, I, V),$$

where a function $e : [0, \infty) \rightarrow [0, \infty)$ is a convex function. We also minimize the terminal cost for ρ_V because maximizing the usage of vaccines is equivalent to minimizing the number of vaccines left at the terminal time T . In this paper, we use a quadratic cost function

$$e_i(t) = \frac{a_i}{2} t^2, \quad (t \in [0, \infty)),$$

where a_i is some constant.

For Item (iv), the cost functional for the concentration of the total population and vaccines can be represented by

$$\int_0^T \mathcal{G}_P(\rho_S(t, \cdot) + \rho_I(t, \cdot) + \rho_R(t, \cdot)) dt, \quad \int_0^T \mathcal{G}_V(\rho_V(t, \cdot)) dt,$$

where

$$(2.6) \quad \mathcal{G}_P(u) = \int_{\Omega} g_P(u(x)) dx, \quad \mathcal{G}_V(u) = \int_{\Omega} g_V(u(x)) dx,$$

for $u : \Omega \rightarrow [0, \infty)$ and convex functions $g_P, g_V : [0, \infty) \rightarrow [0, \infty)$. Similar to e_i from Item (ii), we use quadratic functions for g_P and g_V .

Items (v) and (vi) are criteria specific to the vaccine distribution. From the PDE (2.2), the vaccines are produced during $0 < t < T'$ by a function f . We use the similar functional (2.6) to minimize the amount of vaccines produced by f . We will discuss this functional in detail. Thus, we set the functional

$$\int_0^{T'} \mathcal{G}_0(f(t, \cdot)) dt = \int_0^{T'} \int_{\Omega} g_0(f(t, x)) dx dt$$

where $g_0 : [0, \infty) \rightarrow [0, \infty)$ is a convex function.

The vaccines are delivered during $T' < t < T$. Similar to the Item (i), we set

$$\int_{T'}^T \int_{\Omega} F_V(\rho_V, m_V) dx dt,$$

where F_V has the same definition as (2.5).

The total cost functional we consider is then

$$(2.7) \quad \begin{aligned} \mathcal{P}((\rho_i, m_i)_{i \in \mathbb{S}}, f) &= \sum_{i \in \mathbb{S}} \mathcal{E}_i(\rho_i(T, \cdot)) \\ &+ \int_0^T \int_{\Omega} \sum_{i=S, I, R} F_i(\rho_i, m_i) dx dt + \int_{T'}^T \int_{\Omega} F_V(\rho_V, m_V) dx dt \\ &+ \int_0^T \mathcal{G}_P((\rho_S + \rho_I + \rho_R)(t, \cdot)) + \mathcal{G}_V(\rho_V(t, \cdot)) dt \\ &+ \int_0^{T'} \mathcal{G}_0(f(t, \cdot)) dt. \end{aligned}$$

In the perspective of a control problem, the first line in 2.7 is the final cost, while the rest accounts for the running cost.

In addition to the constraint from (2.3), we adapt the following constraints to reflect the limited vaccination coverage:

$$(2.8) \quad \begin{aligned} 0 &\leq f(t, x) \leq f_{max} & (t, x) &\in [0, T'] \times \Omega_{factory} \\ f(t, x) &= 0 & (t, x) &\in [0, T'] \times \Omega \setminus \Omega_{factory} \\ \rho_V(t, x) &\leq C_{factory} & (t, x) &\in [0, T'] \times \Omega_{factory} \end{aligned}$$

where $\Omega_{factory} \subset \Omega$ indicates the factory area where vaccines are produced and f_{max} is a nonnegative constant that represents the maximum rate of production of vaccines. In the third inequality, a nonnegative constant $C_{factory}$ limits the total number of vaccines produced during $0 < T < T'$.

$$\int_0^{T'} \int_{\Omega} \rho_V(t, x) dx dt \leq C_{factory} T' |\Omega_{factory}|.$$

The constraints (2.8) can be imposed by having the following functionals for \mathcal{G}_V and \mathcal{G}_0 .

$$(2.9) \quad \begin{aligned} \mathcal{G}_V(\rho_V(t, \cdot)) &= \int_{\Omega} g_V(\rho_V(t, x)) dx + i_{\{\rho_V(t, \cdot) \leq C_{factory}\}}(\rho_V(t, \cdot)) \\ \mathcal{G}_0(f(t, \cdot)) &= \int_{\Omega} g_0(f(t, x)) + i_{\Omega_{factory}}(x) f(t, x) dx + i_{\{f(t, \cdot) \leq f_{max}\}}(f(t, \cdot)) \end{aligned}$$

where $\Omega_{factory} \subset \Omega$ indicates the factory area where vaccines are produced. The functionals $i_{\{\rho_V \leq C_{factory}\}}$ and $i_{\{f \leq f_{max}\}}$ are defined as

$$i_{\{u \leq c\}}(u) = \begin{cases} 0, & u(x) \leq c \text{ for all } x \in \Omega \\ \infty, & \text{otherwise} \end{cases}$$

where c is a constant and $u : \Omega \rightarrow \mathbb{R}$ is a function. The function $i_{\Omega_{factory}}(x)$ is defined as

$$i_{\Omega_{factory}}(x) = \begin{cases} 0, & x \in \Omega_{factory} \\ \infty, & x \in \Omega \setminus \Omega_{factory}. \end{cases}$$

This function forces $f(t, x) = 0$ if $(t, x) \in (0, T') \times (\Omega \setminus \Omega_{factory})$, thus vaccines are produced only in $\Omega_{factory}$.

Remark 2.1. The formulation is not limited to SIR epidemic model. For example, we can describe the SIRD (Susceptible-Infected-Recovered-Deceased) epidemic model by adding an extra population ρ_D for the deceased population with a mortality rate μ .

$$\begin{cases} \partial_t \rho_S + \nabla \cdot m_S = -\beta \rho_S K * \rho_I + \frac{\eta_S^2}{2} \Delta \rho_S - \theta_1 \rho_V \rho_S & (t, x) \in (0, T) \times \Omega \\ \partial_t \rho_I + \nabla \cdot m_I = \beta \rho_S K * \rho_I - \gamma \rho_I - \mu \rho_I + \frac{\eta_I^2}{2} \Delta \rho_I & (t, x) \in (0, T) \times \Omega \\ \partial_t \rho_R + \nabla \cdot m_R = \gamma \rho_I + \frac{\eta_R^2}{2} \Delta \rho_R + \theta_1 \rho_V \rho_S & (t, x) \in (0, T) \times \Omega \\ \partial_t \rho_D = \mu \rho_I + \frac{\eta_D^2}{2} \Delta \rho_D & (t, x) \in (0, T) \times \Omega \\ \partial_t \rho_V = f(t, x) - \theta_2 \rho_V \rho_S & (t, x) \in (0, T') \times \Omega \\ \partial_t \rho_V + \nabla \cdot m_V = -\theta_2 \rho_V \rho_S & (t, x) \in [T', T) \times \Omega \end{cases}$$

$\rho_S(0, \cdot), \rho_I(0, \cdot), \rho_R(0, \cdot), \rho_D(0, \cdot), \rho_V(0, \cdot)$ are given.

2.3. Properties. From the definition of the cost functional and the constraint (2.3), we have the following minimization problem:

$$\inf_{(\rho_i, m_i)_{i \in \mathbb{S}}, f} \left\{ \mathcal{P}((\rho_i, m_i)_{i \in \mathbb{S}}, f) : \text{subject to (2.3)} \right\}.$$

We first define the inner product of vectors of functions in L^2 . Given vectors of functions $u = (u_1(t, x), u_2(t, x), \dots, u_k(t, x))$ and $v = (v_1(t, x), v_2(t, x), \dots, v_k(t, x))$ with $u_i, v_i : [0, T] \times \Omega \rightarrow \mathbb{R}$, the L^2 inner product of vectors u and v is defined by

$$(2.10) \quad \langle u, v \rangle_{L^2} = \sum_{i=0}^k (u_i, v_i)_{L^2}$$

where $(\cdot, \cdot)_{L^2}$ is a L^2 inner product such that

$$(u, v)_{L^2} = \int_0^T \int_{\Omega} u(t, x)v(t, x) dx dt.$$

We introduce dual variables $(\phi_i)_{i \in \mathbb{S}}$ for each continuity equation from (2.4). Using the dual variables and the definitions of the inner products, we convert the minimization problem into a saddle point problem.

$$(2.11) \quad \inf_{(\rho_i, m_i)_{i \in \mathbb{S}}, f} \sup_{(\phi_i)_{i \in \mathbb{S}}} \mathcal{L}((\rho_i, m_i, \phi_i)_{i \in \mathbb{S}}, f),$$

where \mathcal{L} is the Lagrangian functional defined as

$$\begin{aligned} & \mathcal{L}((\rho_i, m_i, \phi_i)_{i \in \mathbb{S}}, f) \\ &= \mathcal{P}((\rho_i, m_i)_{i \in \mathbb{S}}, f) - \langle A((\rho_i, m_i)_{i \in \mathbb{S}}, f), (\phi_i)_{i \in \mathbb{S}} \rangle_{L^2} \\ &= \mathcal{P}((\rho_i, m_i)_{i \in \mathbb{S}}, f) \\ &\quad - \int_0^T \int_{\Omega} \phi_S \left(\partial_t \rho_S + \nabla \cdot m_S + \beta \rho_S K * \rho_I + \theta_1 \rho_S \rho_V - \frac{\eta_S^2}{2} \Delta \rho_S \right) dx dt \\ &\quad - \int_0^T \int_{\Omega} \phi_I \left(\partial_t \rho_I + \nabla \cdot m_I - \beta \rho_S K * \rho_I + \gamma \rho_I - \frac{\eta_I^2}{2} \Delta \rho_I \right) dx dt \\ &\quad - \int_0^T \int_{\Omega} \phi_R \left(\partial_t \rho_R + \nabla \cdot m_R - \gamma \rho_I - \theta_1 \rho_S \rho_V - \frac{\eta_R^2}{2} \Delta \rho_R \right) dx dt \\ &\quad - \int_0^T \int_{\Omega} \phi_V \left(\partial_t \rho_V - f \mathcal{X}_{[0, T']}(t) + \nabla \cdot m_V \mathcal{X}_{[T', T]}(t) + \theta_2 \rho_S \rho_V \right) dx dt. \end{aligned}$$

For brevity, we denote

$$u = ((\rho_i, m_i)_{i \in \mathbb{S}}, f), \quad p = (\phi_i)_{i \in \mathbb{S}}.$$

We can rewrite the Lagrangian as

$$(2.12) \quad \mathcal{L}(u, p) = \mathcal{P}(u) - \langle A(u), p \rangle_{L^2}.$$

As noted in [25], the dual gap, the difference between the primal solution and dual solution, may not be zero because the nonconvex functions $(\rho_S, \rho_I) \mapsto \rho_S K * \rho_I$ and

$(\rho_S, \rho_V) \mapsto \rho_S \rho_V$ make the feasible set nonconvex. We circumvent the problem by linearizing the nonlinear operator at a base point \bar{u}

$$A(u) \approx \bar{A}_{\bar{u}}(u) = A(\bar{u}) + [\nabla A(\bar{u})](u - \bar{u}).$$

We define a linearized Lagrangian as

$$(2.13) \quad \bar{\mathcal{L}}_{\bar{u}}(u, p) = \mathcal{P}(u) - \langle \bar{A}_{\bar{u}}(u), p \rangle_{L^2}.$$

In the paper [32], the author developed a primal-dual algorithm using the linearized Lagrangian (Algorithm (3.5)) and proves that the sequence $(u^{(k)}, p^{(k)})_{k=1}^{\infty}$ from the algorithm converges to the saddle point (u_*, p_*) . By the first-order optimality conditions (also known as Karush-Kuhn-Tucker (KKT) conditions), the saddle point satisfies

$$(2.14) \quad \begin{aligned} \partial \mathcal{P}(u_*) - [\nabla A(u_*)]^T p_* &\ni 0 \\ A(u_*) &= 0. \end{aligned}$$

In the Proposition 2.3, we present the properties satisfied by the saddle point, derived from the KKT conditions (2.14). We first recall the definition of the functional derivatives.

DEFINITION 2.2. *Let $F : \mathcal{H} \rightarrow \mathbb{R}$ be a smooth functional where \mathcal{H} is a separable Hilbert space and $\rho : \Omega \rightarrow \mathbb{R}$ be a function in \mathcal{H} . We say a map $\frac{\delta F}{\delta \rho}$ is the functional derivative of F with respect to ρ if it satisfies*

$$\lim_{\epsilon \rightarrow 0} \frac{F(\rho + \epsilon h) - F(\rho)}{\epsilon} = \int_{\Omega} \frac{\delta F}{\delta \rho}(\rho(x)) h(x) dx,$$

for any arbitrary function $h : \Omega \rightarrow \mathbb{R}$.

Now, we show the properties satisfied by the SIRV variational problem.

PROPOSITION 2.3 (Mean-field control SIRV system). *By KKT conditions, the saddle point $((\rho_i, m_i, \phi_i)_{i \in \mathcal{S}}, f)$ of (2.11) satisfies the following equations.*

$$\begin{aligned} \partial_t \phi_S - \frac{\alpha_S}{2} |\nabla \phi_S|^2 + \frac{\eta_S^2}{2} \Delta \phi_S + \frac{\delta \mathcal{G}_P}{\delta \rho}(\rho_S + \rho_I + \rho_R) + \beta(\phi_I - \phi_S) K * \rho_I \\ + \rho_V(\theta_1(\phi_R - \phi_S) - \theta_2 \phi_V) &= 0 & (t, x) \in (0, T) \times \Omega \\ \partial_t \phi_I - \frac{\alpha_I}{2} |\nabla \phi_I|^2 + \frac{\eta_I^2}{2} \Delta \phi_I + \frac{\delta \mathcal{G}_P}{\delta \rho}(\rho_S + \rho_I + \rho_R) \\ + \beta K * (\rho_S(\phi_I - \phi_S)) + \gamma(\phi_R - \phi_I) &= 0 & (t, x) \in (0, T) \times \Omega \\ \partial_t \phi_R - \frac{\alpha_R}{2} |\nabla \phi_R|^2 + \frac{\eta_R^2}{2} \Delta \phi_R + \frac{\delta \mathcal{G}_P}{\delta \rho}(\rho_S + \rho_I + \rho_R) &= 0 & (t, x) \in (0, T) \times \Omega \\ \partial_t \phi_V + \frac{\delta \mathcal{G}_V}{\delta \rho}(\rho_V) + \rho_S(\theta_1(\phi_R - \phi_S) - \theta_2 \phi_V) &= 0 & (t, x) \in (0, T') \times \Omega \\ \partial_t \phi_V - \frac{\alpha_V}{2} |\nabla \phi_V|^2 + \frac{\delta \mathcal{G}_V}{\delta \rho}(\rho_V) + \rho_S(\theta_1(\phi_R - \phi_S) - \theta_2 \phi_V) &= 0 & (t, x) \in (T', T) \times \Omega \\ \partial_t \rho_S - \frac{1}{\alpha_S} \nabla \cdot (\rho_S \nabla \phi_S) + \beta \rho_S K * \rho_I + \theta_1 \rho_S \rho_V - \frac{\eta_S^2}{2} \Delta \rho_S &= 0 & (t, x) \in (0, T) \times \Omega \\ \partial_t \rho_I - \frac{1}{\alpha_I} \nabla \cdot (\rho_I \nabla \phi_I) - \beta \rho_S K * \rho_I + \gamma \rho_I - \frac{\eta_I^2}{2} \Delta \rho_I &= 0 & (t, x) \in (0, T) \times \Omega \end{aligned}$$

$$\begin{aligned}
 \partial_t \rho_R - \frac{1}{\alpha_R} \nabla \cdot (\rho_R \nabla \phi_R) - \gamma \rho_I - \theta_1 \rho_S \rho_V - \frac{\eta_R^2}{2} \Delta \rho_R &= 0 & (t, x) \in (0, T) \times \Omega \\
 \partial_t \rho_V - f + \theta_2 \rho_S \rho_V &= 0 & (t, x) \in (0, T') \times \Omega \\
 \partial_t \rho_V - \frac{1}{\alpha_V} \nabla \cdot (\rho_V \nabla \phi_V) + \theta_2 \rho_S \rho_V &= 0 & (t, x) \in (T', T) \times \Omega \\
 \frac{\delta \mathcal{G}_0}{\delta f}(f) + \phi_V &= 0 & (t, x) \in (0, T') \times \Omega \\
 \phi_i(T, \cdot) &= \frac{\delta \mathcal{E}_i}{\delta \rho(T, \cdot)}(\rho_i(T, \cdot)), \quad i \in \mathbb{S}.
 \end{aligned}$$

The dynamical system models the optimal vector field strategies for S , I , R populations and the vaccine distribution. It combines both strategies from mean field controls and SIRV models. For this reason, we call it *Mean-field control SIRV system*.

The proof of Proposition 2.3 can be found in the Appendix.

3. Algorithms. In this section, we propose an algorithm to solve the proposed SIRV variational problem. We use the primal-dual hybrid gradient (PDHG) algorithm [6, 7]. The PDHG can solve the following convex optimization problem.

$$\begin{aligned}
 \min_u f(Au) + g(u) \\
 \text{subject to } Au = 0
 \end{aligned}$$

where f and g are convex functions and A is a continuous linear operator. The algorithm solves the problem by converting the problem into a saddle point problem by introducing a dual variable p .

$$\min_u \max_p g(u) + \langle Au, p \rangle - f^*(p)$$

where

$$f^*(p) = \sup_u \langle u, p \rangle - f(u)$$

is the Legendre transform of f . The method solves the saddle point problem by iterating

$$\begin{aligned}
 (3.1) \quad u^{(k+\frac{1}{2})} &= \arg \min_u g(u) + \langle u, A^T p^{(k)} \rangle + \frac{1}{2\tau} \|u - u^{(k)}\|_{L^2}^2 \\
 u^{(k+1)} &= 2u^{(k+\frac{1}{2})} - u^{(k)} \\
 p^{(k+1)} &= \arg \max_p \langle Au^{(k+1)}, p \rangle - f^*(p) - \frac{1}{2\sigma} \|p - p^{(k)}\|_{L^2}^2.
 \end{aligned}$$

The scheme converges if the step sizes τ and σ satisfy

$$(3.2) \quad \tau \sigma \|A^T A\|_{L^2} < 1,$$

where $\|\cdot\|$ is an operator norm in L^2 . However, the SIRV variational problem has a nonlinear function A for the constraint. Thus, we use the extension of the algorithm from [32] which solves the nonlinear constrained optimization problem.

$$(3.3) \quad \min_u \max_p g(u) + \langle A(u), p \rangle - f^*(p),$$

where A is a nonlinear constraint. The scheme iterates the algorithm (3.1) with a linear approximation of A at a base point \bar{u}

$$A(u) \approx A(\bar{u}) + [\nabla A(\bar{u})](u - \bar{u}).$$

Thus, we have a linearized saddle point problem

$$(3.4) \quad \min_u \max_p g(u) + \langle A(\bar{u}) + [\nabla A(\bar{u})](x - \bar{u}), p \rangle - f^*(p)$$

and the scheme iterates

$$(3.5) \quad \begin{aligned} u^{(k+\frac{1}{2})} &= \arg \min_u g(u) + \langle u, [\nabla A(u^{(k)})]^T p^{(k)} \rangle + \frac{1}{2\tau^{(k)}} \|u - u^{(k)}\|_{L^2}^2 \\ u^{(k+1)} &= 2u^{(k+\frac{1}{2})} - u^{(k)} \\ p^{(k+1)} &= \arg \max_p \langle A(u^{(k+1)}), p \rangle - f^*(p) - \frac{1}{2\sigma^{(k)}} \|p - p^{(k)}\|_{L^2}^2. \end{aligned}$$

The paper proves that the sequence $\{u^{(k)}, p^{(k)}\}_{k=0}^\infty$ of the algorithm converges to some saddle point (u_*, p_*) that satisfies (2.14). However, the scheme converges if the step sizes satisfy

$$\sigma^{(k)} \tau^{(k)} \|\nabla A(u^{(k)})\|_{L^2}^2 < 1, \quad k = 1, 2, \dots$$

Suppose we use an unbounded operator that depends on the grid size, for example $A = \nabla$. Then the scheme can result in a very slow convergence if we use a fine grid resolution. To circumvent the problem, we use the G-proximal Primal Dual Hybrid Gradient (G-prox PDHG) method from [18] which is another variation of Chambolle-Pock primal dual algorithm. This variant provides an appropriate choice of norms for the algorithm and the authors prove that choosing the proper norms allows the algorithm to have larger step sizes than Chambolle-Pock primal dual algorithm. The G-prox PDHG iterates

$$(3.6) \quad \begin{aligned} u^{(k+\frac{1}{2})} &= \arg \min_u g(u) + \langle u, [\nabla A(u^{(k)})]^T p^{(k)} \rangle + \frac{1}{2\tau^{(k)}} \|u - u^{(k)}\|_{L^2}^2 \\ u^{(k+1)} &= 2u^{(k+\frac{1}{2})} - u^{(k)} \\ p^{(k+1)} &= \arg \max_p \langle A(u^{(k+1)}), p \rangle - f^*(p) - \frac{1}{2\sigma^{(k)}} \|p - p^{(k)}\|_{\mathcal{H}^{(k)}}^2. \end{aligned}$$

where the norm $\|\cdot\|_{\mathcal{H}^{(k)}}$ is defined as

$$\|u\|_{\mathcal{H}^{(k)}}^2 = \|[\nabla A(u^{(k)})]^T u\|_{L^2}^2.$$

By choosing the proper norms, the step sizes only need to satisfy

$$\sigma^{(k)} \tau^{(k)} < 1, \quad k = 1, 2, \dots$$

which are clearly independent of the grid size.

3.1. Implementation of the algorithm. To implement the algorithm to the minimization problem (2.7), we set

$$\begin{aligned} u &= ((\rho_i, m_i)_{i \in \mathbb{S}}, f) \\ p &= (\phi_i)_{i \in \mathbb{S}} \\ g(u) &= \mathcal{P}(u) \\ f(A(u)) &= \begin{cases} 0 & \text{if } A(u) = 0 \\ \infty & \text{otherwise} \end{cases} \\ f^*(p) &= 0. \end{aligned}$$

We use (2.4) for the definition of the operator A .

$$A(u) = (A_S(u), A_I(u), A_R(u), A_V(u))$$

$$\begin{aligned} A_S(u) &= \partial_t \rho_S + \nabla \cdot m_S - \frac{\eta_S^2}{2} \Delta \rho_S + \beta \rho_S K * \rho_I + \theta_1 \rho_S \rho_V, \\ A_I(u) &= \partial_t \rho_I + \nabla \cdot m_I - \frac{\eta_I^2}{2} \Delta \rho_I - \beta \rho_I K * \rho_S + \gamma \rho_I, \\ A_R(u) &= \partial_t \rho_R + \nabla \cdot m_R - \frac{\eta_R^2}{2} \Delta \rho_R, \\ A_V(u) &= \partial_t \rho_V - f \mathcal{X}_{[0, T']}(t) + \nabla \cdot m_V \mathcal{X}_{[T', T]}(t) + \theta_1 \rho_S \rho_V. \end{aligned}$$

Define the Lagrangian functional as

$$\mathcal{L}x := \mathcal{P}(x) - \langle A(u), p \rangle_{L^2}$$

where $\langle \cdot, \cdot \rangle_{L^2}$ is defined in (2.10). We summarize the algorithm as follows.

Algorithm 1: G-prox PDHG for mean-field control SIRV system

Input: $\rho_i(0, \cdot)$ ($i \in \mathbb{S}$)

Output: ρ_i, m_i, ϕ_i ($i \in \mathbb{S}$), f

While relative error $>$ tolerance **for** $i \in \mathbb{S}$

$$\begin{aligned} \rho_i^{(k+1)} &= \arg \min_{\rho} \mathcal{L}((\rho, m^{(k)}, f^{(k)}), \phi^{(k)}) + \frac{1}{2\tau} \|\rho - \rho_i^{(k)}\|_{L^2}^2 \\ m_i^{(k+1)} &= \arg \min_m \mathcal{L}((\rho^{(k+1)}, m, f^{(k)}), \phi_i^{(k)}) + \frac{1}{2\tau} \|m - m_i^{(k)}\|_{L^2}^2 \\ f^{(k+1)} &= \arg \min_f \mathcal{L}((\rho^{(k+1)}, m^{(k+1)}, f), \phi^{(k)}) + \frac{1}{2\tau} \|f - f^{(k)}\|_{L^2}^2 \\ \phi_i^{(k+\frac{1}{2})} &= \arg \max_{\phi} \mathcal{L}((\rho^{(k+1)}, m^{(k+1)}, f^{(k+1)}), \phi) - \frac{1}{2\sigma} \|\phi - \phi_i^{(k)}\|_{H_i^{(k)}}^2 \\ \phi_i^{(k+1)} &= 2\phi_i^{(k+\frac{1}{2})} - \phi_i^{(k)} \end{aligned}$$

Here, L^2 and $H_i^{(k)}$ norms are defined as

$$\|u\|_{L^2}^2 = (u, u)_{L^2} = \int_0^T \int_{\Omega} u^2 dx dt, \quad \|u\|_{H_i^{(k)}}^2 = \|[\nabla A_i(u^{(k)})]^T u\|_{L^2}^2, \quad i \in \mathbb{S}$$

for any $u : [0, T] \times \Omega \rightarrow [0, \infty)$. Moreover, the relative error is defined as

$$\text{relative error} = \frac{|\mathcal{P}(\rho_i^{(k+1)}, m_i^{(k+1)}) - \mathcal{P}(\rho_i^{(k)}, m_i^{(k)})|}{|\mathcal{P}(\rho_i^{(k)}, m_i^{(k)})|}.$$

In the section 4, We use quadratic functions for \mathcal{E}_i ($i \in \{S, I, V\}$), \mathcal{G}_P , \mathcal{G}_V , \mathcal{G}_0 . With the definitions (2.9), we use

$$\begin{aligned}\mathcal{E}_i(\rho_i(T, \cdot)) &= \int_{\Omega} \frac{a_i}{2} \rho_i(T, x)^2 dx, \quad i = S, I, V \\ \mathcal{G}_P(\rho(t, \cdot)) &= \int_{\Omega} \frac{d_P}{2} \rho(t, x)^2 dx \\ \mathcal{G}_V(\rho(t, \cdot)) &= \int_{\Omega} \frac{d_V}{2} \rho(t, x)^2 dx + i_{\{\rho(t, \cdot) \leq C_{factory}\}}(\rho(t, \cdot)) \\ \mathcal{G}_0(f(t, \cdot)) &= \int_{\Omega} \frac{d_0}{2} f(t, x)^2 + i_{\Omega_{factory}}(x) f(t, x) dx + i_{\{f(t, \cdot) \leq f_{max}\}}(f(t, \cdot))\end{aligned}$$

Thus, we can write the cost functional as follows

$$\begin{aligned}(3.7) \quad \mathcal{P}((\rho_i, m_i)_{i \in \mathbb{S}}, f) &= \int_{\Omega} \sum_{i=S, I, V} \frac{a_i}{2} \rho_i(T, \cdot)^2 dx \\ &+ \int_0^T \int_{\Omega} \sum_{i=S, I, R} F_i(\rho_i, m_i) dx dt + \int_{T'}^T \int_{\Omega} F_V(\rho_V, m_V) dx dt \\ &+ \int_0^T \int_{\Omega} \frac{d_P}{2} (\rho_S + \rho_I + \rho_R)^2 + \frac{d_V}{2} \rho_V^2 dx dt \\ &+ \int_0^{T'} \int_{\Omega} \frac{d_0}{2} f^2 + i_{\Omega_{factory}} f dx dt \\ &+ \int_0^T i_{\{\rho(t, \cdot) \leq C_{factory}\}}(\rho(t, \cdot)) + i_{\{f(t, \cdot) \leq f_{max}\}}(f(t, \cdot)) dt\end{aligned}$$

where a_i , d_P , d_V , d_0 are nonnegative constants. With this cost functional, we find explicit formula for each variable $\rho_i^{(k+1)}$, $m_i^{(k+1)}$, $\phi_i^{(k+1)}$ ($i \in \mathbb{S}$), $f^{(k+1)}$.

PROPOSITION 3.1. *The variables $\rho_i^{(k+1)}$, $m_i^{(k+1)}$, $\phi_i^{(k+1)}$ ($i \in \mathbb{S}$), and $f^{(k+1)}$ from the Algorithm 1 satisfy the following explicit formulas:*

$$\begin{aligned}\rho_S^{(k+1)} &= root_+ \left(\frac{\tau}{1 + \tau d_P} \left(\partial_t \phi_S^{(k)} + \frac{\eta_S^2}{2} \Delta \phi_S^{(k)} - \frac{1}{\tau} \rho_S^{(k)} + \beta \left(\phi_I^{(k)} - \phi_S^{(k)} \right) K * \rho_I^{(k)} \right. \right. \\ &\quad \left. \left. + \rho_V^{(k)} \left(\theta_1(\phi_R^{(k)} - \phi_S^{(k)}) - \theta_2 \phi_V^{(k)} \right) + d_P(\rho_I^{(k)} + \rho_R^{(k)}) \right), 0, -\frac{\tau \alpha_S |m_S^{(k)}|^2}{2(1 + \tau d_P)} \right) \\ \rho_I^{(k+1)} &= root_+ \left(\frac{\tau}{1 + \tau d_P} \left(\partial_t \phi_I^{(k)} + \frac{\eta_I^2}{2} \Delta \phi_I^{(k)} - \frac{1}{\tau} \rho_I^{(k)} + \beta K * \left(\rho_S^{(k)} (\phi_I^{(k)} - \phi_S^{(k)}) \right) \right. \right. \\ &\quad \left. \left. + \gamma(\phi_R^{(k)} - \phi_I^{(k)}) + d_P(\rho_S^{(k)} + \rho_R^{(k)}) \right), 0, -\frac{\tau \alpha_I |m_I^{(k)}|^2}{2(1 + \tau d_P)} \right) \\ \rho_R^{(k+1)} &= root_+ \left(\frac{\tau}{1 + \tau d_P} \left(\partial_t \phi_R^{(k)} + \frac{\eta_R^2}{2} \Delta \phi_R^{(k)} - \frac{1}{\tau} \rho_R^{(k)} + d_P(\rho_S^{(k)} + \rho_I^{(k)}) \right), 0, -\frac{\tau \alpha_R |m_R^{(k)}|^2}{2(1 + \tau d_P)} \right) \\ \rho_V^{(k+1)} &= \min \left(C_{factory}, \frac{\tau}{1 + \tau d_V} \left(-\partial_t \phi_V^{(k)} - \rho_S^{(k)} (\theta_1(\phi_R^{(k)} - \phi_S^{(k)}) - \theta_2 \phi_V^{(k)}) + \frac{1}{\tau} \rho_V^{(k)} \right) \right), \\ &\quad (t, x) \in [0, T'] \times \Omega\end{aligned}$$

$$\rho_V^{(k+1)} = \text{root}_+ \left(\frac{\tau}{1 + \tau d_V} \left(\partial_t \phi_V^{(k)} + \rho_S (\theta_1 (\phi_R - \phi_S) - \theta_2 \phi_V) - \frac{1}{\tau} \rho_V^{(k)} \right), 0, -\frac{\tau \alpha_V |m_V^{(k)}|^2}{2(1 + \tau d_V)} \right),$$

$$(t, x) \in (T', T] \times \Omega$$

$$m_i^{(k+1)} = \frac{\rho_i^{(k+1)}}{\tau \alpha_i + \rho_i^{(k+1)}} \left(m_i^{(k)} - \tau \nabla \phi_i^{(k)} \right), \quad (i \in \mathbb{S})$$

$$f^{(k+1)} = \min \left(f_{max}, \frac{\tau}{1 + \tau d_0} \left(\frac{1}{\tau} f^{(k)} - \phi_V^{(k)} \right) \right) \mathcal{X}_{\Omega_{factory}}(x)$$

$$\phi_S^{(k+\frac{1}{2})} = \phi_S^{(k)} + \sigma (A_S A_S^T)^{-1} \left(-\partial_t \rho_S^{(k+1)} - \nabla \cdot m_S^{(k+1)} - \beta \rho_S^{(k+1)} K * \rho_I^{(k+1)} - \theta_1 \rho_S^{(k+1)} \rho_V^{(k+1)} + \frac{\eta_S^2}{2} \Delta \rho_S^{(k+1)} \right)$$

$$\phi_I^{(k+\frac{1}{2})} = \phi_I^{(k)} + \sigma (A_I A_I^T)^{-1} \left(-\partial_t \rho_I^{(k+1)} - \nabla \cdot m_I^{(k+1)} + \beta \rho_S^{(k+1)} K * \rho_I^{(k+1)} - \gamma \rho_I^{(k+1)} + \frac{\eta_I^2}{2} \Delta \rho_I^{(k+1)} \right)$$

$$\phi_R^{(k+\frac{1}{2})} = \phi_R^{(k)} + \sigma (A_R A_R^T)^{-1} \left(-\partial_t \rho_R^{(k+1)} - \nabla \cdot m_R^{(k+1)} + \gamma \rho_I^{(k+1)} + \theta_1 \rho_S^{(k+1)} \rho_V^{(k+1)} + \frac{\eta_R^2}{2} \Delta \rho_R^{(k+1)} \right)$$

$$\phi_V^{(k+\frac{1}{2})} = \phi_V^{(k)} + \sigma (A_V A_V^T)^{-1} \left(-\partial_t \rho_V^{(k+1)} + f^{(k+1)} \mathcal{X}_{[0, T']}(t) - \nabla \cdot m_V^{(k+1)} \mathcal{X}_{[T', T]}(t) - \theta_1 \rho_S^{(k+1)} \rho_V^{(k+1)} \right)$$

where $\text{root}_+(a, b, c)$ is a positive root of a cubic polynomial $x^3 + ax^2 + bx + c = 0$ and we approximate the $A_i A_i^T$ as follows

$$\begin{aligned} A_S A_S^T &= -\partial_{tt} + \frac{\eta_S^4}{4} \Delta^2 - (1 + (\beta + \theta_1) \eta_S^2) \Delta + (\beta + \theta_1)^2 \\ A_I A_I^T &= -\partial_{tt} + \frac{\eta_I^4}{4} \Delta^2 - (1 + (\gamma + \beta) \eta_I^2) \Delta + (\gamma + \beta)^2 \\ A_R A_R^T &= -\partial_{tt} + \frac{\eta_R^4}{4} \Delta^2 - \Delta \\ A_V A_V^T &= -\partial_{tt} - \Delta + \theta_2^2. \end{aligned}$$

We use FFTW library to compute $(A_i A_i^T)^{-1}$ ($i \in \mathbb{S}$) and convolution terms by Fast Fourier Transform (FFT), which is $O(n \log n)$ operations per iteration with n being the number of points. Thus, the algorithm takes just $O(n \log n)$ operations per iteration.

4. Experiments. In this section, we present several sets of numerical experiments using the algorithm 1 with various parameters. We wrote C++ codes to run the numerical experiments. Let $\Omega = [0, 1]^2$ be a unit square in \mathbb{R}^2 and the terminal time $T = 1$. The domain $[0, T] \times \Omega$ is discretized with the regular Cartesian grid below.

$$\Delta x_1 = \frac{1}{N_{x_1}}, \quad \Delta x_2 = \frac{1}{N_{x_2}}, \quad \Delta t = \frac{1}{N_t - 1}$$

$$\begin{aligned} x_{kl} &= ((k + 0.5) \Delta x_1, (l + 0.5) \Delta x_2), \quad k = 0, \dots, N_{x_1} - 1, \quad l = 0, \dots, N_{x_2} - 1 \\ t_n &= n \Delta t, \quad n = 0, \dots, N_t - 1 \end{aligned}$$

where N_x, N_y are the number of discretized points in space and N_t is the number of discretized points in time. For all the experiments, we use the same set of parameters,

$$\begin{aligned} N_{x_1} &= 128, \quad N_{x_2} = 128, \quad N_t = 32 \\ \alpha_S &= 10, \quad \alpha_I = 30, \quad \alpha_R = 20, \quad \alpha_V = 0.005 \end{aligned}$$

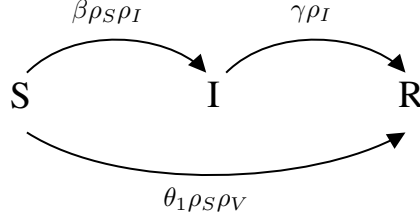


Fig. 1: Visualization of the flow of three populations. The susceptible transforms to the infected with a rate β and the recovered with a rate θ_1 . The infected transforms to the recovered with a rate γ .

$$\begin{aligned} a_S = 2, \quad a_I = 2, \quad a_R = 0.001, \quad a_V = 0.1 \\ T' = 0.5, \quad \sigma = 0.01, \quad d_P = 0.4, \quad d_V = 0.4, \quad d_0 = 0.01 \\ \theta_2 = 0.9 \quad \eta_i = 0.01 \quad (i \in \mathbb{S}). \end{aligned}$$

By setting a higher value for α_I , we penalize the infected population's movement more than other populations. Considering the immobility of the infected individuals, this is a reasonable choice in terms of real-world applications. By setting $T' = 1/2$, the solution will produce the vaccines during $0 \leq t < 1/2$ and deliver them during $1/2 \leq t \leq 1$. Furthermore, we fix the parameters for the infection rate and recovery rate

$$\beta = 0.8, \quad \gamma = 0.1.$$

The paper [25] describes how the parameters β and γ affect the propagation of the populations. In this paper, we focus on the vaccine distributions. Recall that from the formulation (3.7), we have terminal functionals

$$\mathcal{E}_i(\rho_i(T, \cdot)) = \int_{\Omega} \frac{a_i}{2} \rho_i(T, x)^2 dx, \quad i \in \{S, I, V\}.$$

Thus, the solution to the problem has to minimize the total number of susceptible, infected, and vaccines at the terminal time T . The solution reduces the total number of infected by recovering them with a rate γ and decreases the total number of susceptible by transforming the susceptible to the infected with a rate β or to the recovered with a rate θ_1 (Figure 1). If the β is large and γ is small, there are more inflows from susceptible to the infected than the outflow to the recovered from the infected. To minimize the total number of the infected, the solution has to vaccinate the susceptible as much as possible to avoid the susceptible becoming infected. Thus, the vaccines need to be produced and delivered to the susceptible efficiently while satisfying the constraint conditions (2.8).

We present two experiments that demonstrate how the various factors in the formulation affect the production and the distribution of vaccines.

4.1. Experiment 1. In this experiment, we show how the parameters related to ρ_V affect the solution. We set the initial densities for the ρ_i ($i \in \mathbb{S}$) and the factory

location $\Omega_{factory}$ as

$$(4.1) \quad \begin{aligned} \rho_S(0, x) &= (2 \exp(-5[(x_1 - 0.7)^2 + (x_2 - 0.7)^2]) - 1.5)_+ \\ \rho_I(0, x) &= (2 \exp(-5[(x_1 - 0.7)^2 + (x_2 - 0.7)^2]) - 1.8)_+ \\ \rho_R(0, x) &= 0 \\ \rho_V(0, x) &= 0 \\ \Omega_{factory} &= B_{0.1}(0.3, 0.3) \end{aligned}$$

where $(x)_+ = \max(x, 0)$ and $B_r x$ is a ball of a radius r centered at x .

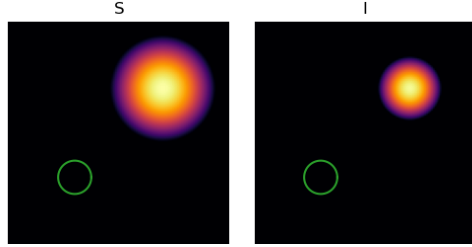


Fig. 2: Experiment 1: Initial densities of ρ_S and ρ_I . The green circle indicates $\Omega_{factory}$.

With the initial densities (4.1), we run two simulations with different values for θ_1 , θ_2 , and f_{max} .

Parameters	Sim 1	Sim 2	Description
θ_1	0.5	0.9	Vaccine efficiency
f_{max}	0.5	10	Maximum production rate of vaccines
$C_{factory}$	0.5	2	Maximum amount of vaccines that can be produced at $x \in \Omega$ during $0 \leq t \leq T'$

The Figure 3 shows the comparison between the results from the simulation 1 and the simulation 2. The first three plots (Figure 3a) show the total mass of ρ_i ($i = S, I, R$), i.e.

$$\int_{\Omega} \rho_i(t, x) dx, \quad i = S, I, R, \quad t \in [0, T].$$

and the last plot (Figure 3b) shows the total mass of ρ_V during $0 \leq t \leq T'$

$$\int_{\Omega} \rho_V(t, x) dx, \quad t \in [0, T'].$$

The total number of vaccines produced from the simulation 1 is smaller than that from the simulation 2 because the solution cannot produce a large amount of vaccines due to the low production rate f_{max} . Furthermore, the solution from the simulation 1 cannot vaccinate a large number of susceptible due to a small θ_1 . Thus, there are more susceptible and less recovered at the terminal time in the simulation 1.

4.2. Experiment 2. In this experiment, we show how the obstacles in the spatial domain affects the production and distribution of the vaccines. Denote a set $\Omega_{obs} \subset \Omega$ as obstacles. We use the following functionals in the experiment.

$$\mathcal{G}_i(\rho(t, \cdot)) = \int_{\Omega} \frac{d_i}{2} \rho^2(t, x) + i_{\Omega_{obs}}(x) \rho(t, x) dx, \quad i \in \{P, V\}$$

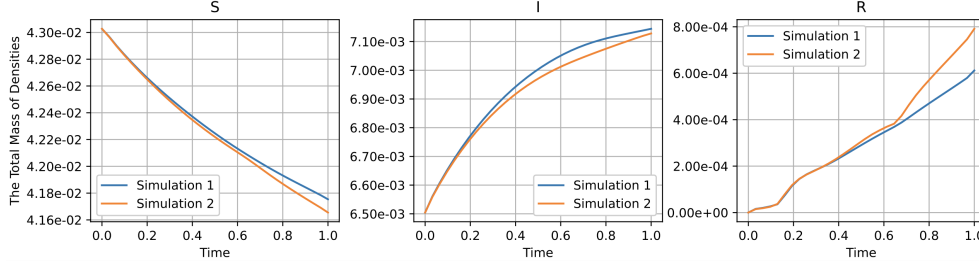
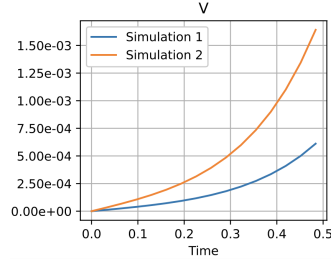
(a) The total population of ρ_S, ρ_I, ρ_R .(b) The total mass of vaccines produced during $0 \leq t \leq T'$.

Fig. 3: Experiment 1: The comparison between the results from the simulation 1 and the simulation 2. The first three plots (A) show the total mass of ρ_i ($i = S, I, R$) and the fourth plot (B) demonstrates the total mass of ρ_V produced at the factory area during the production time $0 \leq t < T'$.

$$\begin{aligned} \mathcal{E}_i(\rho(T, \cdot)) &= \int_{\Omega} \frac{a_i}{2} \rho^2(T, x) + i_{\Omega_{obs}}(x) \rho(T, x) dx, \quad i \in \{S, I, V\} \\ \mathcal{E}_R(\rho(T, \cdot)) &= \int_{\Omega} \frac{a_R}{2} (\rho(T, x) - 1)^2 + i_{\Omega_{obs}}(x) \rho(T, x) dx. \end{aligned}$$

The densities ρ_i ($i \in \mathbb{S}$) cannot be positive on Ω_{obs} due to $i_{\Omega_{obs}}$. Thus, the densities transport while avoiding the obstacle Ω_{obs} . We set the initial densities and $\Omega_{factory}$ as follows

$$\begin{aligned} \rho_S(0, x) &= (2 \exp(-15((x_1 - 0.2)^2 + (x_2 - 0.5)^2)) - 1.6)_+ \\ &\quad + (2 \exp(-15((x_1 - 0.8)^2 + (x_2 - 0.5)^2)) - 1.6)_+ \\ \rho_I(0, x) &= (2 \exp(-15((x_1 - 0.2)^2 + (x_2 - 0.5)^2)) - 1.8)_+ \\ \rho_R(0, x) &= 0 \\ \rho_V(0, x) &= 0 \\ \Omega_{factory} &= B_{0.075}(0.5, 0.5) \end{aligned}$$

and fix the parameters

$$\theta_1 = 0.9, \quad f_{max} = 10, \quad C_{factory} = 2.$$

The initial densities are shown in Figure 4.

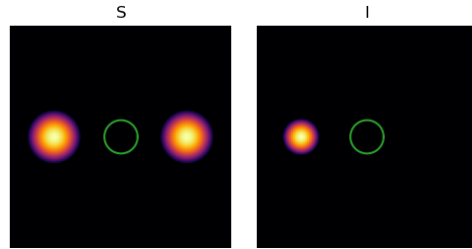


Fig. 4: Experiment 2: The initial densities ρ_S and ρ_I , and the location of the factory (indicated as a green circle).

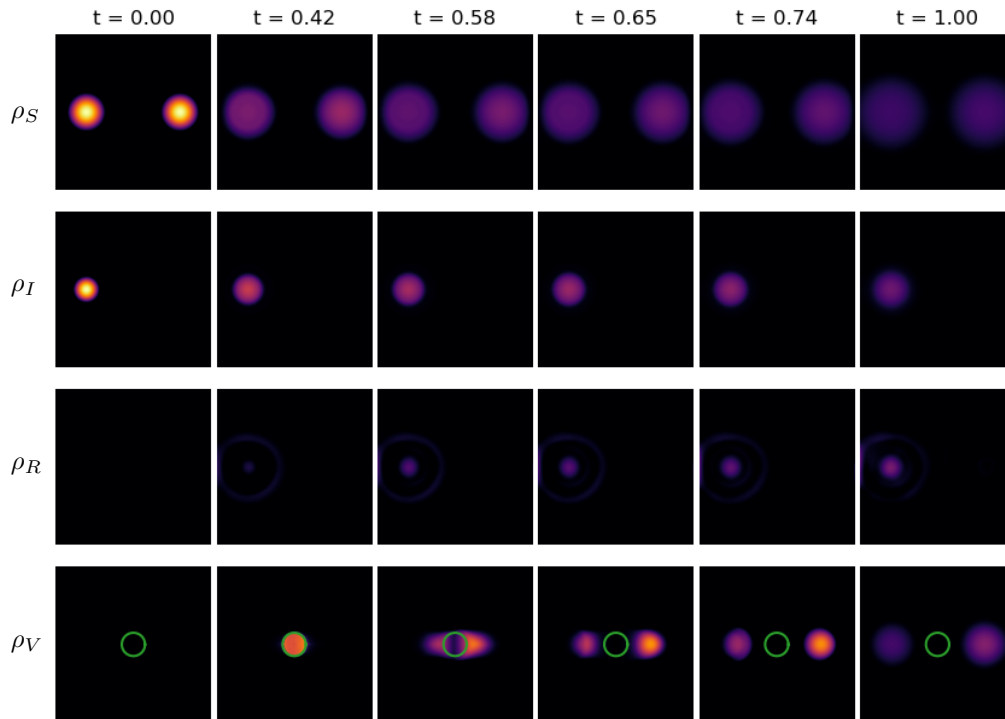


Fig. 5: Experiment 2: The evolution of densities ρ_i ($i \in \mathbb{S}$) without the obstacle over time $0 \leq t \leq 1$. The first row: the susceptible density ρ_S . The second row: the infected density ρ_I . The third row: the recovered density ρ_R . The fourth row: the vaccine density ρ_V .

The Figure 5 and Figure 6 show the evolution of densities with and without obstacles, respectively. In both simulations, the density of vaccines ρ_V (the fourth row) transports to the areas where the susceptible people are present. In Figure 6, ρ_V transports while avoiding the obstacle at the right. Figure 7 shows the comparison between these two solutions and how the presence of the obstacle affects the produc-

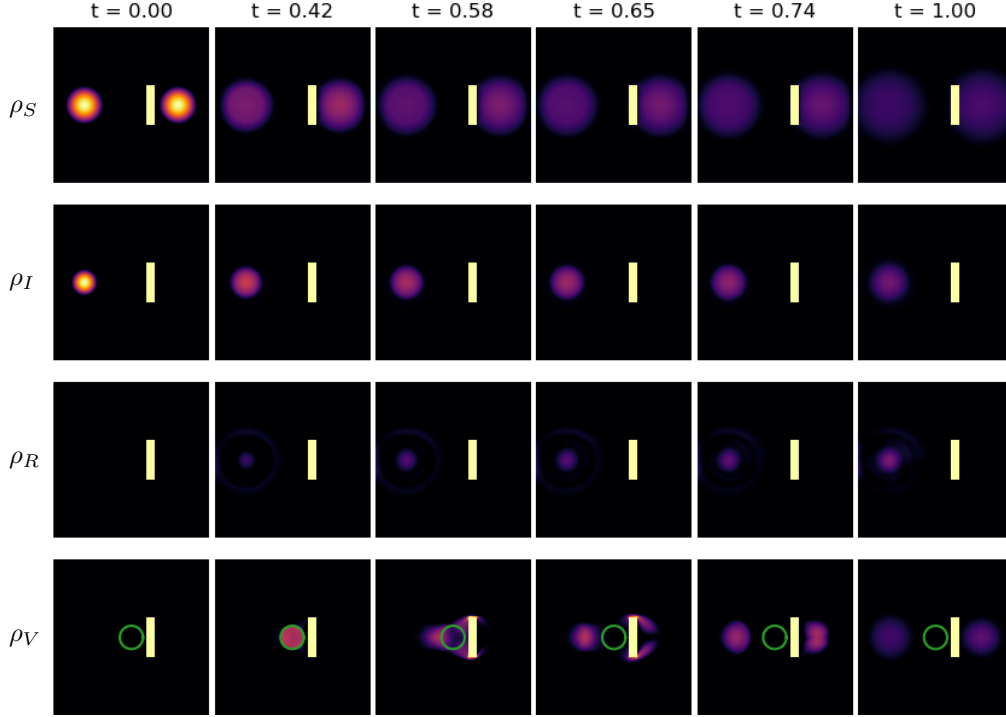


Fig. 6: Experiment 2: The evolution of densities ρ_i ($i \in \mathbb{S}$) with the obstacle (indicated as a yellow block) over time $0 \leq t \leq 1$. The first row: the susceptible density ρ_S . The second row: the infected density ρ_I . The third row: the recovered density ρ_R . The fourth row: the vaccine density ρ_V .

tion and delivery of vaccines quantitatively. Figure 7a shows the total mass of the vaccines in the factory area $\Omega_{factory}$ during the production time

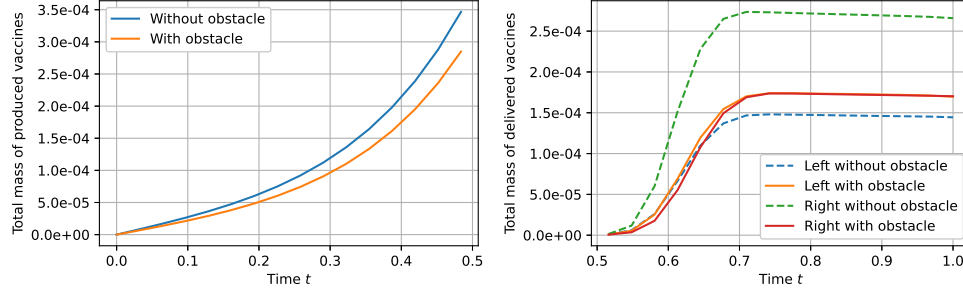
$$\int_{\Omega_{factory}} \rho_V(t, x) dx, \quad t \in [0, T'].$$

Figure 7b shows the total mass of the vaccines during the delivery time at the left side and the right side of the domain

$$\begin{aligned} & \int_{\Omega \cap \{x_1 < 0.5\}} \rho_V(t, x) dx, \quad \text{Left} \\ & \int_{\Omega \cap \{x_1 \geq 0.5\}} \rho_V(t, x) dx, \quad \text{Right} \end{aligned}$$

during $t \in [T', T]$. When there is no obstacle, the vaccines are delivered more to the right than to the left (Figure 7b). The number of susceptible people at the left decreases very fast because there are infected people with a high infection rate. When ρ_V starts to transport at time $t = T'$, the number of susceptible is lower at the left.

Thus, the solution distributes fewer vaccines to the left with less susceptible people. When there is an obstacle, ρ_V has to bypass the obstacle to reach the susceptible areas. Thus, the kinetic energy cost during the delivery time $t \in [T', T]$ increases at the right. The solution cannot deliver the vaccines as much as the case without the obstacle. It results in a fewer number of vaccines produced during $t \in [0, T')$ (Figure 7a) and delivered to the right during $t \in [T', T]$ when there is an obstacle (Figure 7b).



(a) The total mass of ρ_V during $t \in [0, 0.5]$ (b) The total mass of ρ_V during $t \in [0.5, 1]$

Fig. 7: Experiment 3: The left plot shows the total mass of vaccine density ρ_V during the production time $t \in [0, T')$. The right plot shows the total mass of ρ_V at the left side of the domain $\Omega \cap \{x_1 < 0.5\}$ and at the right side of the domain $\Omega \cap \{x_1 \geq 0.5\}$.

4.3. Experiment 3. Similar to Experiment 2, we show how the obstacles in the spatial domain affect the production and distribution of the vaccines. We use more complex initial densities, an obstacle set Ω_{obs} , and three factory locations in this experiment. We set the initial densities and $\Omega_{factory}$ as follows

$$\begin{aligned}
 \rho_S(0, x) &= (2 \exp(-15((x_1 - 0.8)^2 + (x_2 - 0.8)^2)) - 1.6)_+ \\
 &\quad + (2 \exp(-15((x_1 - 0.2)^2 + (x_2 - 0.7)^2)) - 1.6)_+ \\
 &\quad + (2 \exp(-15((x_1 - 0.8)^2 + (x_2 - 0.3)^2)) - 1.6)_+ \\
 &\quad + (2 \exp(-15((x_1 - 0.2)^2 + (x_2 - 0.2)^2)) - 1.6)_+ \\
 \rho_I(0, x) &= (2 \exp(-15((x_1 - 0.2)^2 + (x_2 - 0.7)^2)) - 1.8)_+ \\
 &\quad + (2 \exp(-15((x_1 - 0.2)^2 + (x_2 - 0.2)^2)) - 1.8)_+ \\
 \rho_R(0, x) &= 0 \\
 \rho_V(0, x) &= 0 \\
 \Omega_{factory} &= B_{0.075}(0.5, 0.2) \cup B_{0.075}(0.5, 0.5) \cup B_{0.075}(0.5, 0.8)
 \end{aligned}$$

and fix the parameters

$$\theta_1 = 0.9, \quad f_{max} = 10, \quad C_{factory} = 2.$$

The initial densities are shown in Figure 4.

The Figure 9 and Figure 10 show the evolution of densities with and without obstacles, respectively. The experiment demonstrates that even with the complex

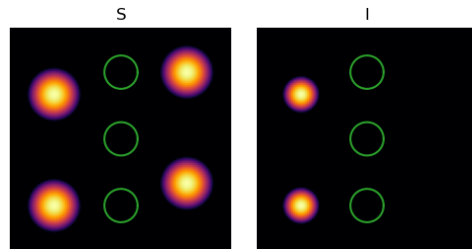


Fig. 8: Experiment 3: The initial densities ρ_S and ρ_I , and the location of the factory (indicated as green circles).

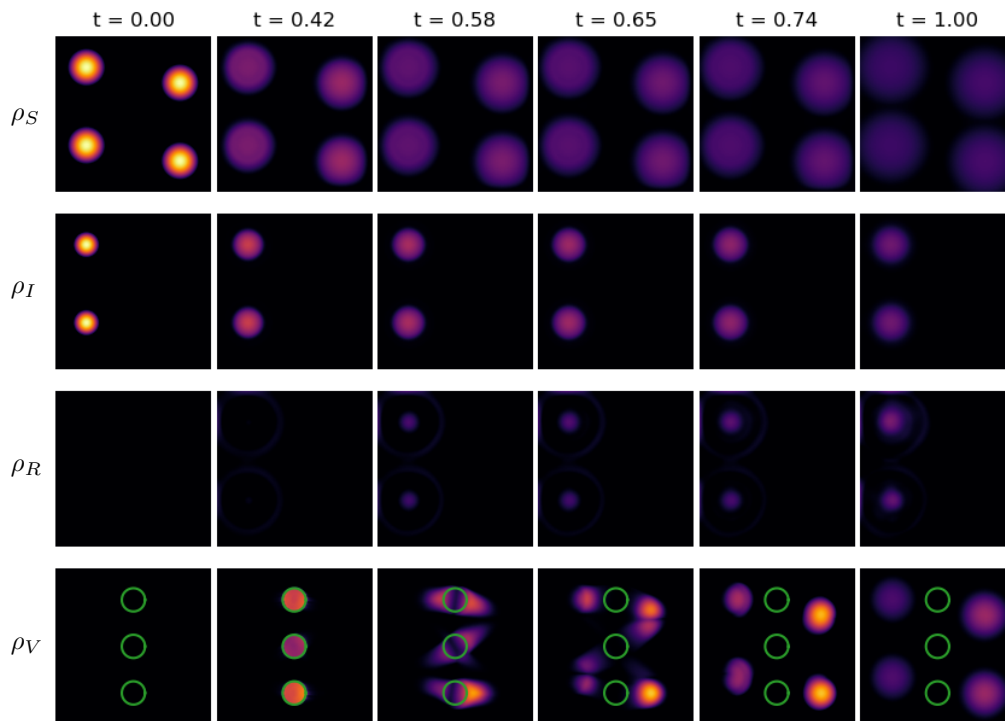


Fig. 9: Experiment 3: The evolution of densities ρ_i ($i \in \mathbb{S}$) without the obstacle over time $0 \leq t \leq 1$. The first row: the susceptible density ρ_S . The second row: the infected density ρ_I . The third row: the recovered density ρ_R . The fourth row: the vaccine density ρ_V .

initial densities, the algorithm successfully converges to the reasonable solution that coincides with the previous experiments. The density of vaccines ρ_V (the fourth row) transports to the areas where the susceptible people are present while avoiding the obstacles.

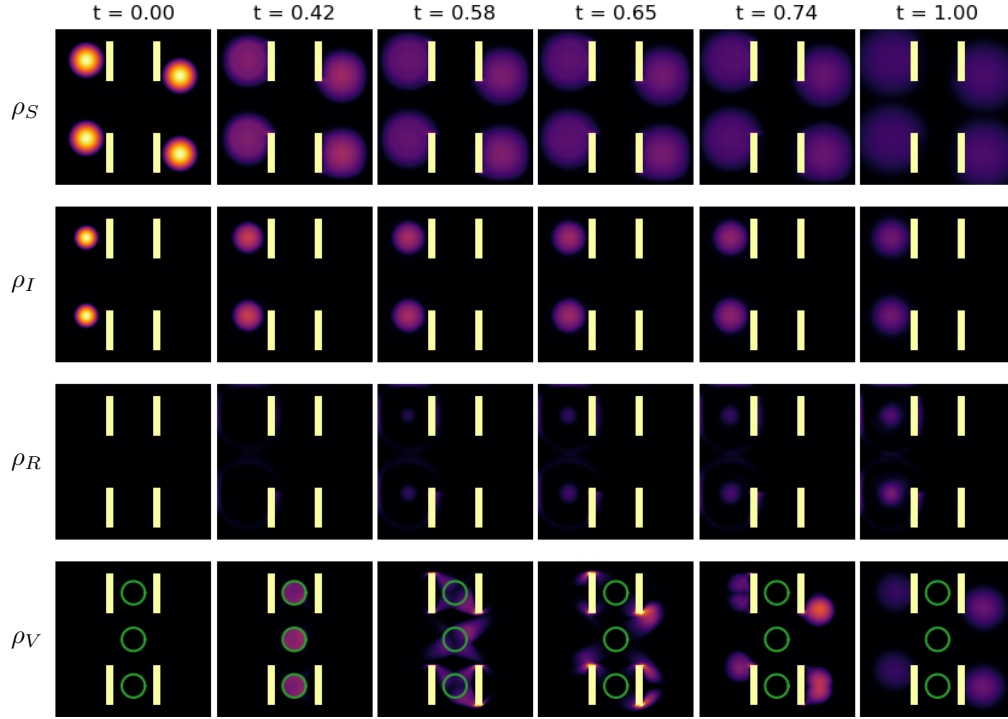


Fig. 10: Experiment 3: The evolution of densities ρ_i ($i \in \mathbb{S}$) with the obstacle (indicated as yellow blocks) over time $0 \leq t \leq 1$. The first row: the susceptible density ρ_S . The second row: the infected density ρ_I . The third row: the recovered density ρ_R . The fourth row: the vaccine density ρ_V .

Figure 11a shows the total mass of the vaccines produced during the production time at each factory location. Without the obstacles, the total mass of ρ_V at the middle is the lowest at time T' because the factory at the middle is the farthest away from the susceptible people. It is more efficient to produce the vaccines at the factories closer to the susceptible (the top and the bottom factories) to reduce the kinetic energy cost during the delivery time $T \in [T', T]$. However, with the obstacles, the vaccines are produced the most at the middle factory. Since the obstacles are blocking the paths between the top and the bottom factories and the susceptible people, ρ_V has to bypass them to reach to the target area. The pathways from the middle factory to the susceptible people are not blocked as much as from the top and the bottom factories. Thus, it is more efficient to produce more vaccines at the middle factory.

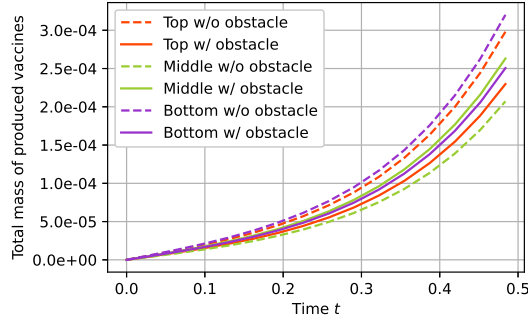
Figure 11b shows the total mass of the vaccines during the delivery time at dif-

ferent locations. The lines in the plot represent the following quantities:

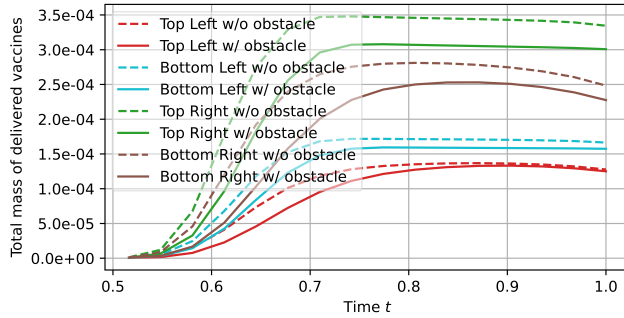
$$\int_{\Omega \cap \{x_1 < 0.5\} \cap \{x_2 \geq 0.5\}} \rho_V(t, x) dx, \quad \text{Top Left} \quad \int_{\Omega \cap \{x_1 \geq 0.5\} \cap \{x_2 \geq 0.5\}} \rho_V(t, x) dx, \quad \text{Top Right}$$

$$\int_{\Omega \cap \{x_1 < 0.5\} \cap \{x_2 < 0.5\}} \rho_V(t, x) dx, \quad \text{Bottom Left} \quad \int_{\Omega \cap \{x_1 \geq 0.5\} \cap \{x_2 < 0.5\}} \rho_V(t, x) dx, \quad \text{Bottom Right}$$

over $t \in [T', T]$. With the obstacles, the kinetic energy cost increases since ρ_V has to bypass to reach to the targets when it transports from the top and the bottom factories. As a result, the vaccines are not produced as much as the simulation without the obstacles, and there are less vaccines reached to the targets.



(a) The total mass of ρ_V during $t \in [0, 0.5]$



(b) The total mass of ρ_V during $t \in [0.5, 1]$

Fig. 11: Experiment 3: The top plot shows the total mass of vaccine density ρ_V at three factory locations during the production time $t \in [0, T']$. The bottom plot shows the total mass of ρ_V at the top left area of the domain $\Omega \cap \{x_1 < 0.5\} \cap \{x_2 \geq 0.5\}$, at the bottom left area $\Omega \cap \{x_1 < 0.5\} \cap \{x_2 < 0.5\}$, at the top right area $\Omega \cap \{x_1 \geq 0.5\} \cap \{x_2 \geq 0.5\}$, and at the bottom right area $\Omega \cap \{x_1 \geq 0.5\} \cap \{x_2 < 0.5\}$ during the distribution time $t \in [T', T]$.

5. Discussion. In this paper, we formulate a class of mean-field control problems for distributing vaccines in a spatial domain. We build a macroscopic variational model with a vaccine distribution parameter to control the number of suspected, infected, and recovered populations. This model forms a constrained optimal control

problem in unnormalized density spaces. Numerically, we demonstrate that the proposed model helps distribute the vaccine efficiently. Here the efficiency is built by the mean-field cost functional, which models both the transportation cost and the vaccine's effectiveness.

6. Appendix.

Proof of Proposition 2.3. From the saddle point problem (2.11), we can rewrite the problem as

$$(6.1) \quad \inf_{(\rho_i, m_i)_{i \in \mathbb{S}}, f} \sup_{\phi} \mathcal{P}((\rho_i, m_i)_{i \in \mathbb{S}}, f) - \int_0^T \int_{\Omega} \sum_{i \in \{S, I, R\}} \phi_i \left(\partial_t \rho_i + \nabla \cdot m_i - \frac{\eta_i^2}{2} \Delta \rho_i \right) dx dt \\ + \int_0^T \mathcal{Q}((\rho_i, \phi_i)_{i \in \mathbb{S}}) dt - \int_0^T \int_{\Omega} \phi_V \partial_t \rho_V dx dt + \int_0^{T'} \int_{\Omega} f \phi_V dx dt - \int_{T'}^T \int_{\Omega} \phi_V \nabla \cdot m_V dx dt$$

where a function $\mathcal{Q} : (0, T) \times \Omega \rightarrow \mathbb{R}$ is defined as

$$\mathcal{Q}((\rho_i, \phi_i)_{i \in \mathbb{S}}) = \int_{\Omega} \beta \rho_S (\phi_I - \phi_S) K * \rho_I + \gamma \rho_I (\phi_R - \phi_I) + \rho_S \rho_V (\theta_1 (\phi_R - \phi_S) - \theta_2 \phi_V) dx.$$

If $((\rho_i, m_i, \phi_i)_{i \in \mathbb{S}}, f)$ is the saddle point of the problem, the differential of Lagrangian with respect to ρ_i, m_i, ϕ_i ($i \in \mathbb{S}$), f and $\rho_i(T, \cdot)$ ($i \in \{S, I, V\}$) equal to zero. Thus, from $\frac{\delta \mathcal{L}}{\delta \phi_i} = 0$ we have

$$\partial_t \rho_i + \nabla \cdot m_i - \frac{\eta_i^2}{2} \Delta \rho_i + \frac{\delta \mathcal{Q}}{\delta \phi_i}((\rho_i, \phi_i)_{i \in \mathbb{S}}) = 0 \quad (t, x) \in (0, T) \times \Omega, \quad i = S, I, R \\ \partial_t \rho_V - f + \frac{\delta \mathcal{Q}}{\delta \phi_V}((\rho_i, \phi_i)_{i \in \mathbb{S}}) = 0 \quad (t, x) \in (0, T') \times \Omega \\ \partial_t \rho_V + \nabla \cdot m_V + \frac{\delta \mathcal{Q}}{\delta \phi_V}((\rho_i, \phi_i)_{i \in \mathbb{S}}) = 0 \quad (t, x) \in (T', T) \times \Omega.$$

Using integration by parts, we reformulate the Lagrangian function (6.1) as follows.

$$\mathcal{L}((\rho_i, m_i, \phi_i)_{i \in \mathbb{S}}, f) \\ = \sum_{i \in \mathbb{S}} \mathcal{E}_i(\rho_i(T, \cdot)) + \int_0^T \mathcal{G}_P(\rho_S + \rho_I + \rho_R) + \mathcal{G}_V(\rho_V) dt + \int_0^{T'} \mathcal{G}_0(f(t, \cdot)) dt \\ + \sum_{i=S, I, R} \int_0^T \int_{\Omega} \frac{\alpha_i |m_i|^2}{2 \rho_i} + m_i \cdot \nabla \phi_i + \frac{\eta_i^2}{2} \rho_i \Delta \phi_i dx dt + \sum_{i \in \mathbb{S}} \int_0^T \int_{\Omega} \rho_i \partial_t \phi_i dx dt \\ + \int_{T'}^T \int_{\Omega} \frac{\alpha_V |m_V|^2}{2 \rho_V} + m_V \cdot \nabla \phi_V dx dt + \int_0^{T'} \int_{\Omega} f \phi_V dx dt + \int_0^T \mathcal{Q}((\rho_i, \phi_i)_{i \in \mathbb{S}}) dt \\ + \sum_{i=S, I, R, V} \int_{\Omega} \rho_i(0, x) \phi_i(0, x) - \rho_i(T, x) \phi_i(T, x) dx$$

From $\frac{\delta \mathcal{L}}{\delta \rho_i} = 0$ ($i \in \{S, I, R\}$),

$$\frac{\delta \mathcal{G}_P}{\delta \rho_i}(\rho_S + \rho_I + \rho_R) + \frac{\delta \mathcal{Q}}{\delta \rho_i}((\rho_i, \phi_i)_{i \in \mathbb{S}}) - \frac{\alpha_i |m_i|^2}{2 \rho_i^2} + \frac{\eta_i^2}{2} \Delta \phi_i + \partial_t \phi_i = 0 = 0 \quad (t, x) \in (0, T) \times \Omega$$

From $\frac{\delta \mathcal{L}}{\delta \rho_V} = 0$,

$$\begin{aligned} \frac{\delta \mathcal{G}_V}{\delta \rho_V}(\rho_V) + \frac{\delta \mathcal{Q}}{\delta \rho_V}((\rho_i, \phi_i)_{i \in \mathbb{S}}) + \partial_t \phi_V &= 0 \quad (t, x) \in (0, T') \times \Omega \\ \frac{\delta \mathcal{G}_V}{\delta \rho_V}(\rho_V) + \frac{\delta \mathcal{Q}}{\delta \rho_V}((\rho_i, \phi_i)_{i \in \mathbb{S}}) - \frac{\alpha_V |m_V|^2}{2\rho_V^2} + \partial_t \phi_V &= 0 \quad (t, x) \in (T', T) \times \Omega. \end{aligned}$$

From $\frac{\delta \mathcal{L}}{\delta \rho_i(T, \cdot)} = 0$ ($i \in \mathbb{S}$),

$$\frac{\delta \mathcal{E}}{\delta \rho_i(T, \cdot)}(\rho_i(T, \cdot)) = \phi_i(T, \cdot).$$

From $\frac{\delta \mathcal{L}}{\delta f} = 0$,

$$\frac{\delta \mathcal{G}_0}{\delta f}(f) + \phi_V = 0, \quad (t, x) \in (0, T') \times \Omega.$$

From $\frac{\delta \mathcal{L}}{\delta m_i} = 0$ ($i \in \mathbb{S}$),

$$\begin{aligned} \frac{\alpha_i m_i}{\rho_i} &= -\nabla \phi_i \quad (t, x) \in (0, T) \times \Omega, \quad i \in \{S, I, R\} \\ \frac{\alpha_V m_V}{\rho_V} &= -\nabla \phi_V \quad (t, x) \in (0, T') \times \Omega. \end{aligned}$$

By replacing $\frac{\alpha_i m_i}{\rho_i} = -\nabla \phi_i$ in $\frac{\delta \mathcal{L}}{\delta \rho_i} = 0$ and $\frac{\delta \mathcal{L}}{\delta \phi_i} = 0$, we derive the result. \square

REFERENCES

- [1] Y. ACHDOU AND I. CAPUZZO-DOLCETTA, *Mean field games: numerical methods*, SIAM Journal on Numerical Analysis, 48 (2010), pp. 1136–1162.
- [2] Y. ACHDOU AND M. LAURIÈRE, *Mean field games and applications: Numerical aspects*, arXiv preprint arXiv:2003.04444, (2020).
- [3] A. AURELL, R. CARMONA, G. DAYANIKLI, AND M. LAURIÈRE, *Optimal incentives to mitigate epidemics: a stackelberg mean field game approach*, arXiv preprint arXiv:2011.03105, (2020).
- [4] A. BENSOUSSAN, T. HUANG, AND M. LAURIÈRE, *Mean field control and mean field game models with several populations*, arXiv preprint arXiv:1810.00783, (2018).
- [5] L. BRICEÑO-ARIAS, D. KALISE, Z. KOBEISSI, M. LAURIÈRE, A. M. GONZÁLEZ, AND F. J. SILVA, *On the implementation of a primal-dual algorithm for second order time-dependent mean field games with local couplings*, ESAIM: Proceedings and Surveys, 65 (2019), pp. 330–348.
- [6] A. CHAMBOLLE AND T. POCK, *A first-order primal-dual algorithm for convex problems with applications to imaging*, J. Math. Imaging Vision, 40 (2011), pp. 120–145, <https://doi.org/10.1007/s10851-010-0251-1>, <https://doi.org/10.1007/s10851-010-0251-1>.
- [7] A. CHAMBOLLE AND T. POCK, *On the ergodic convergence rates of a first-order primal-dual algorithm*, Math. Program., 159 (2016), pp. 253–287, <https://doi.org/10.1007/s10107-015-0957-3>, <https://doi.org/10.1007/s10107-015-0957-3>.
- [8] A. CHARPENTIER, R. ELIE, M. LAURIÈRE, AND V. C. TRAN, *Covid-19 pandemic control: balancing detection policy and lockdown intervention under icu sustainability*, Mathematical Modelling of Natural Phenomena, 15 (2020), p. 57.
- [9] M. CIRANT, *Multi-population mean field games systems with neumann boundary conditions*, Journal de Mathématiques Pures et Appliquées, 103 (2015), pp. 1294–1315.
- [10] L. DI DOMENICO, G. PULLANO, C. E. SABBATINI, P.-Y. BOËLLE, AND V. COLIZZA, *Impact of lockdown on covid-19 epidemic in île-de-france and possible exit strategies*, BMC medicine, 18 (2020), pp. 1–13.
- [11] G. DIMARCO, B. PERTHAME, G. TOSCANI, AND M. ZANELLA, *Social contacts and the spread of infectious diseases*, arXiv preprint arXiv:2009.01140, (2020).
- [12] J. DONCEL, N. GAST, AND B. GAUJAL, *A mean field game analysis of sir dynamics with vaccination*, Probability in the Engineering and Informational Sciences, (2020), pp. 1–18.

- [13] E. FELEQI, *The derivation of ergodic mean field game equations for several populations of players*, Dynamic Games and Applications, 3 (2013), pp. 523–536.
- [14] S. FLAXMAN, S. MISHRA, A. GANDY, H. J. T. UNWIN, T. A. MELLAN, H. COUPLAND, C. WHITTAKER, H. ZHU, T. BERAH, J. W. EATON, ET AL., *Estimating the effects of non-pharmaceutical interventions on covid-19 in europe*, Nature, 584 (2020), pp. 257–261.
- [15] P. GODARA, S. HERMINGHAUS, AND K. M. HEIDEMANN, *A control theory approach to optimal pandemic mitigation*, PloS one, 16 (2021), p. e0247445.
- [16] E. HANSEN AND T. DAY, *Optimal control of epidemics with limited resources*, Journal of mathematical biology, 62 (2011), pp. 423–451.
- [17] M. HUANG, R. P. MALHAMÉ, AND P. E. CAINES, *Large population stochastic dynamic games: closed-loop mckean-vaslov systems and the nash certainty equivalence principle*, Communications in Information & Systems, 6 (2006), pp. 221–252.
- [18] M. JACOBS, F. LÉGER, W. LI, AND S. OSHER, *Solving Large-Scale Optimization Problems with a Convergence Rate Independent of Grid Size*, arXiv:1805.09453 [math], (2018), <https://arxiv.org/abs/1805.09453>.
- [19] J. JANG, H.-D. KWON, AND J. LEE, *Optimal control problem of an sir reaction-diffusion model with inequality constraints*, Mathematics and Computers in Simulation, 171 (2020), pp. 136–151.
- [20] M. KANTNER AND T. KOPRUCKI, *Beyond just “flattening the curve”: Optimal control of epidemics with purely non-pharmaceutical interventions*, Journal of Mathematics in Industry, 10 (2020), pp. 1–23.
- [21] J. KIM, H.-D. KWON, AND J. LEE, *Constrained optimal control applied to vaccination for influenza*, Computers & Mathematics with Applications, 71 (2016), pp. 2313–2329.
- [22] L. LAGUZET AND G. TURINICI, *Individual vaccination as nash equilibrium in a sir model with application to the 2009–2010 influenza a (h1n1) epidemic in france*, Bulletin of Mathematical Biology, 77 (2015), pp. 1955–1984.
- [23] J.-M. LASRY AND P.-L. LIONS, *Mean field games*, Japanese journal of mathematics, 2 (2007), pp. 229–260.
- [24] W. LEE, R. LAI, W. LI, AND S. OSHER, *Generalized unnormalized optimal transport and its fast algorithms*, Journal of Computational Physics, (2021), p. 110041.
- [25] W. LEE, S. LIU, H. TEMBINE, W. LI, AND S. OSHER, *Controlling propagation of epidemics via mean-field games*, arXiv preprint arXiv:2006.01249, (2020).
- [26] G. B. LIBOTTE, F. S. LOBATO, G. M. PLATT, AND A. J. S. NETO, *Determination of an optimal control strategy for vaccine administration in covid-19 pandemic treatment*, Computer methods and programs in biomedicine, 196 (2020), p. 105664.
- [27] J. LIU AND X.-S. WANG, *Optimal allocation of face masks during the covid-19 pandemic: a case study of the first epidemic wave in the united states*, arXiv preprint arXiv:2101.03023, (2020).
- [28] B. M. NDIAYE, L. TENDENG, AND D. SECK, *Analysis of the covid-19 pandemic by sir model and machine learning technics for forecasting*, arXiv preprint arXiv:2004.01574, (2020).
- [29] L. RUTHOTTO, S. J. OSHER, W. LI, L. NURBEKYAN, AND S. W. FUNG, *A machine learning framework for solving high-dimensional mean field game and mean field control problems*, Proceedings of the National Academy of Sciences, 117 (2020), pp. 9183–9193.
- [30] J. L. SESTERHENN, *Adjoint-based data assimilation of an epidemiology model for the Covid-19 pandemic in 2020*, arXiv preprint arXiv:2003.13071, (2020).
- [31] C. J. SILVA, C. CRUZ, D. F. TORRES, A. P. MUÑOZURI, A. CARBALLOSA, I. AREA, J. J. NIETO, R. FONSECA-PINTO, R. PASSADOURO, E. S. DOS SANTOS, ET AL., *Optimal control of the covid-19 pandemic: controlled sanitary deconfinement in portugal*, Scientific reports, 11 (2021), pp. 1–15.
- [32] T. VALKONEN, *A primal-dual hybrid gradient method for nonlinear operators with applications to MRI*, Inverse Problems, 30 (2014), pp. 055012, 45, <https://doi.org/10.1088/0266-5611/30/5/055012>, <https://doi.org/10.1088/0266-5611/30/5/055012>.
- [33] G. ZAMAN, Y. H. KANG, AND I. H. JUNG, *Stability analysis and optimal vaccination of an sir epidemic model*, BioSystems, 93 (2008), pp. 240–249.